Intermetallics 96 (2018) 94–103

Contents lists available at ScienceDirect

Intermetallics

journal homepage: www.elsevier.com/locate/intermet

A comparative study of the rate effect on deformation mode in ductile and brittle bulk metallic glasses

Ding Zhou[a,b], Bing Hou[a,b], Bingjin Li[a,b], Shuangyin Zhang[a,b], Lanhong Dai[c], Yulong Li[a,b,*]

[a] Institute of Advanced Materials and Structures, Northwestern Polytechnical University, Xi'an, 710072, China
[b] School of Aeronautics, Northwestern Polytechnical University, Xi'an, 710072, China
[c] State Key Laboratory of Nonlinear Mechanics, Institute of Mechanics, Chinese Academy of Sciences, Beijing, 100190, China

ARTICLE INFO

Keywords:
Metallic glass
Rate effect
Deformation mode
Ductile
Brittle

ABSTRACT

The rate effect on the deformation mode of bulk metallic glasses (BMGs) is investigated by a comparative study between ductile and brittle compositions via real-time photographing. The strain-rate controls the deformation mode transition from shear-dominated sliding under quasi-static compression to cracking-dominated fracture under dynamic compression. In ductile BMGs, progressive sliding occurs at lower strain rate and contributes to a stable deformation manner. In brittle BMGs, however, unstable deformation occurs through rapid sliding even under quasi-static compression. Both ductile and brittle BMGs undergo unstable deformation under dynamic compression. The rate-dependent and composition-dependent tendency of stable or unstable deformation is well characterized by a model based on the ratio of the applied strain energy to the critical dissipation energy at the local shear banding region.

1. Introduction

The coexistence of macroscopically brittle failure and being capable of considerable plastic shear flow at microscale in metallic glasses leads to complicated deformation modes under various loading conditions. It is well accepted that the plastic deformation of bulk metallic glasses (BMGs) is accommodated by shear banding [1–6]. The multiplication and intersection of shear bands contribute to a stable deformation manner [7,8]. However, the catastrophic failure also originates from shear instability within shear bands [9–13]. Thus, the various deformation modes in BMGs are determined by different shear banding behaviors. Extensive reports have shown that the shear banding behaviors and hereby deformation modes are influenced by various factors, including material compositions [14–16], loading rate [17–24] and temperature [25–28]. In addition, sample size [29–31] and stress state during loading [32,33] also affect deformation mode.

Among these factors, loading rate is considered as one of the most significant since metallic glasses are applied to areas over a wide range of strain rate. Zeng et al. [23] reported a shear-dominated failure under quasi-static compression, while a fragmental fracture under dynamic compression. The flow serrations during plastic flow was suggested to be related to shear stability [34], and the serrations gradually disappeared with increasing strain rate [35,36]. Mukai et al. [17] proposed BMGs occurred progressive sliding at lower loading rate, while rapid sliding at higher rate. These findings indicate a transition from stable deformation to unstable deformation with increasing loading rate. However, some compositions exhibit unstable failure even at a low strain rate [4,20]. Thus, a systematic study of how rate-effect controls the deformation mode in different compositions is needed.

In the present study, we have investigated the strain-rate effect on the deformation mode in ductile and brittle BMGs under quasi-static and dynamic compression. $Zr_{65}Cu_{18}Ni_7Al_{10}$ (short for Zr65-BMGs) and $Zr_{50}Cu_{40}Al_{10}$ (short for Zr50-BMGs) bulk metallic glasses were selected as model materials for ductile and brittle BMGs, respectively. Real-time photographing and scan electronic microscope (SEM) observation were utilized to relate the mechanical responses to specific shear banding or cracking behaviors. The results showed the tendency of stable deformation or unstable deformation originates from different shear banding and cracking behaviors during softening process. Such tendency showed both rate dependence and composition dependence. A model from the energy-dissipation perspective was introduced to reveal how rate-effect controlled deformation mode in ductile and brittle BMGs.

2. Materials and methods

Monolithic $Zr_{65}Cu_{18}Ni_7Al_{10}$ and $Zr_{50}Cu_{40}Al_{10}$ (at %) BMGs were prepared by arc-melting a mixture of corresponding pure compositions

* Corresponding author. Institute of Advanced Materials and Structures, Northwestern Polytechnical University, Xi'an, 710072, China.
E-mail address: liyulong@nwpu.edu.cn (Y. Li).

https://doi.org/10.1016/j.intermet.2018.01.020
Received 26 December 2017; Received in revised form 24 January 2018; Accepted 28 January 2018
Available online 20 March 2018
0966-9795/

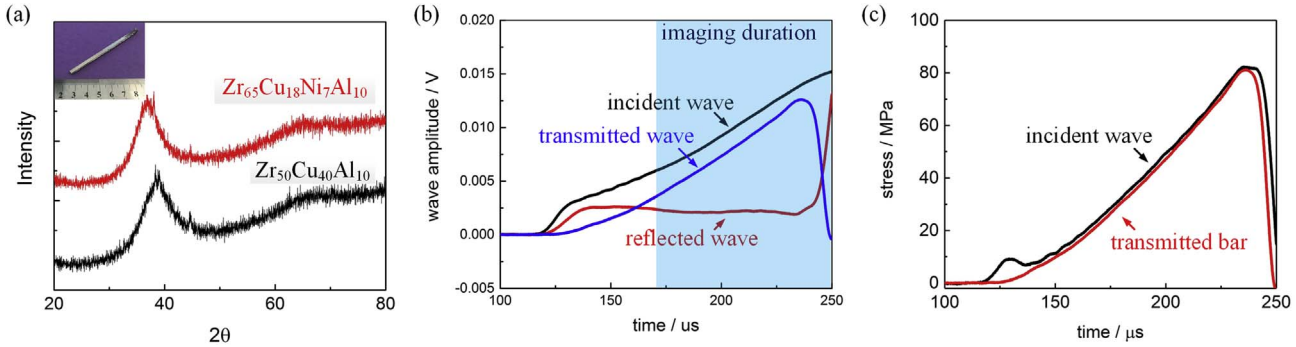

Fig. 1. (a) XRD patterns of Zr65-BMG and Zr50-BMG. Inset is the alloy ingot. (b) Typical incident, reflected and transmitted wave under dynamic loading. The image duration (the blue area) is set to cover the first impulse during loading. (c) The stresses on the incident and transmitted bar during the first impulse, indicating the stress equilibrium is guaranteed in the specimen. (For interpretation of the references to colour in this figure legend, the reader is referred to the Web version of this article.)

(99.9%) in a Ti-gettered argon atmosphere. The master alloy ingots were re-melted six times to ensure homogeneity, which was then injected into a water-cooled copper mold to fabricate rectangle ingots (see the inset of Fig. 1a). The amorphous nature of the ingots was confirmed by X-ray diffraction (XRD) (Fig. 1a). Rectangle samples with a cross section of 3 × 3 mm were cut from the ingots. The aspect ratio of the specimens is 2:1 under quasi-static compression, and 1:1 under dynamic compression. Both ends of the samples were polished to ensure surface parallelism.

Quasi-static compressive tests were performed by a CRIMS DNS-100 hydraulic testing machine. The loading rates were set at 5×10^{-4} s^{-1} and 5×10^{-3} s^{-1}. Dynamic compressive tests were performed by split Hopkinson pressure bar (SHPB) with loading rates of 300 s^{-1} and 1000 s^{-1}. Typical wave signals under dynamic loading were shown in Fig. 1b. The stress equilibrium in the specimen was guaranteed during the first impulse (Fig. 1c). Real-time deformation processes under quasi-static and dynamic loading were captured by high-speed cameras. Under dynamic loading, the high-speed camera was triggered by the first rising edge of the incident wave, ensuring the capture of deformation process during the first impulse (see the imaging duration in Fig. 1b). For each testing sample, its one surface was polished to be a mirror surface in order to capture shear banding and cracking behaviors. At least six samples were tested for each condition to exclude occasional cases. The fracture samples were observed by a scan electronic microscopy (SEM, ZEISS SUPRA 55).

3. Results

3.1. Stress-strain curves under quasi-static and dynamic compression

The stress-strain curves of Zr65-BMGs under quasi-static and dynamic compression are shown in Fig. 2a. The Zr65-BMGs show considerable plasticity with serrated flow under quasi-static compression, which corresponds to a stable deformation manner. It is worthy to mention that the sample of 5×10^{-4} s^{-1} is unloaded before catastrophic fracture, but it is obvious that Zr65-BMGs can keep stable deformation at a much larger strain under lower loading rate. However, the stress-strain curves under dynamic loading show merely approximate elastic loading and sudden stress-drop without serrated flow. This indicates a brittle failure under dynamic loading, and a transition from stable deformation to unstable deformation with increasing strain rate. Different from Zr65-BMGs, Zr50-BMGs show limited plasticity under both quasi-static and dynamic loading (Fig. 2b). This implies the rate effect on the deformation mode might not be obvious in Zr50-BMGs. To further investigate the deformation modes of both ductile and brittle BMGs under various loading conditions, the real-time deformation images are synchronized with the corresponding mechanical responses.

3.2. Shear banding and cracking behaviors in ductile BMGs

Fig. 3 shows the stress-strain curves and characteristic shear banding behaviors of Zr65-BMGs under quasi-static compression. The stress-strain curves can be divided into three stage, i.e., elastic deformation, work-hardening stage and softening stage (Fig. 3a1 and a2). At the end of the work-hardening stages, a number of shear bands are observed on the imaging surface of the Zr65-BMG samples (Fig. 3b1 and b2). This indicates the formation of multiple shear bands occurs during work-hardening. Fig. 3c1 and c2 shows preferential slip planes originate from existed shear bands during the softening stage under 5×10^{-4} s^{-1} and 5×10^{-3} s^{-1}, respectively. Comparing Fig. 3c1 and d1 (or c2 and d2), one can see progressive sliding occurs along the slip planes in a stable manner. The stick-slip motion was suggested to

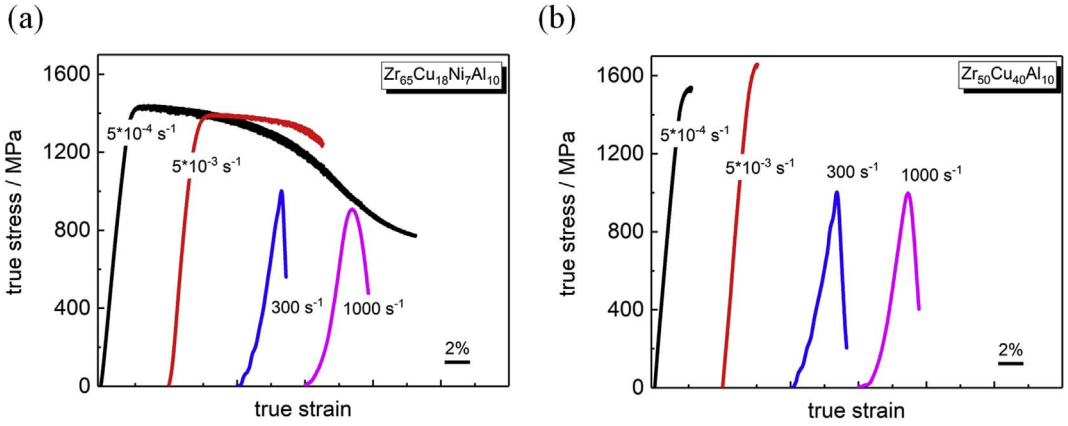

Fig. 2. Stress-strain curves of (a) ductile (Zr65-BMGs) and (b) brittle (Zr50-BMGs) under quasi-static and dynamic compression.

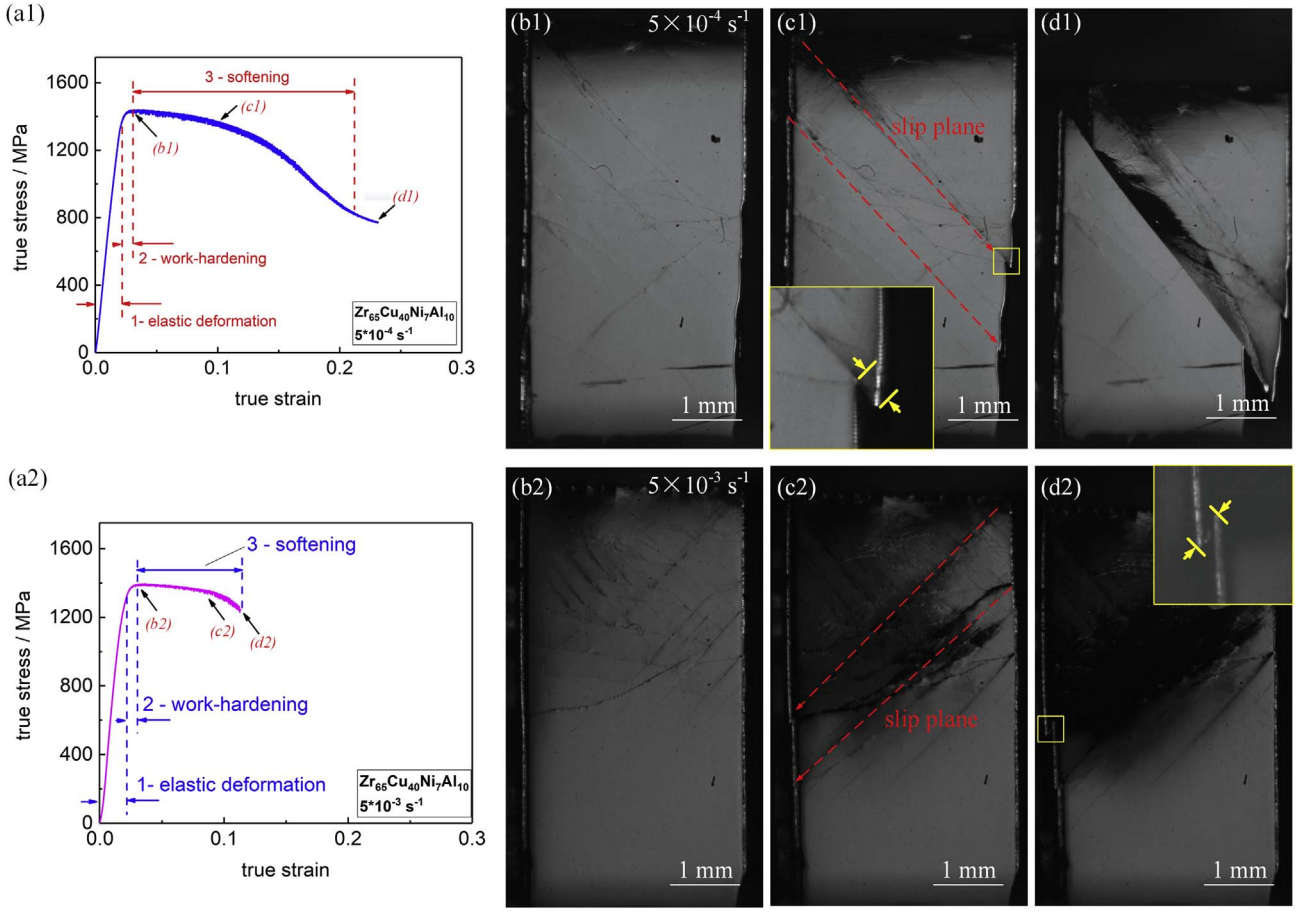

Fig. 3. Stress-strain curves of Zr65-BMGs under (a1) 5×10^{-4} s^{-1} and (a2) 5×10^{-3} s^{-1}. Characteristic shear banding behaviors of 5×10^{-4} s^{-1}, including (b1) multiple shear banding, (c1) formation of slip planes and (d1) extensive secondary shear banding; and (b2) – (d2) shear banding operations of 5×10^{-3} s^{-1}.

correspond to serrated flow, and to be related to shear stability in BMGs [34,37,38]. Meanwhile, extensive secondary shear bands initiate and propagate between the slip planes. This implies that the serrated flow and thereby stable deformation are not merely resulted from progressive sliding along slip planes. Instead, the alternant occurrence of progressive sliding and secondary shear banding might be the governing cause for stable deformation manner. Although Zr65-BMG exhibit stable deformation manner under both 5×10^{-4} s^{-1} and 5×10^{-3} s^{-1}, the displacement of stable deformation decreases with increasing strain rate.

Fig. 4 shows the mechanical responses and characteristic deformation behaviors of Zr65-BMGs under dynamic compression. The stress-time curve shows an approximately elastic loading and a direct softening without plastic flow, which is quite different from that under quasi-static compression (Fig. 3). The initiation of a single shear band is observed during the loading stage under 300 s^{-1} and 1000 s^{-1} in Fig. 4 b1 and b2, respectively. Several shear band branches can be observed in along the single shear band (Fig. 4c2). It is intriguing that a crack directly initiates from the single shear band, rather than formation of multiple shear bands (Fig. 4c1 and d2). The initiation of a crack also corresponds to a direct transition from loading stage to softening stage. This is followed by the initiation and propagation of another crack (Fig. 4e1 and e2). The characteristic deformation images reveal that Zr65-BMGs undergo cracking right after single shear banding under dynamic compression, which leads to an unstable deformation manner. This is quite different from the multiple shear banding and the stable sliding under quasi-static compression.

The shear band patterns and fracture morphologies of Zr65-BMGs are further observed by SEM in Fig. 5. A number of major shear bands (Fig. 5a1 and a2) and extensive secondary shear bands (Fig. 5b1 and b2) are observed on the imaging surfaces of the fractured samples under quasi-static loading, which confirms the images captured by real-time photographing (Fig. 3). Considering the Zr65-BMG sample does not undergo catastrophic failure under 5×10^{-4} s^{-1}, we take a top-view of the slip plane (Fig. 5c1). It is interesting that only shearing traces and several shear bands are observed on the slip plane (Fig. 5d1), which is quite different from the classical fracture surfaces covered by vein-like patterns [10,19,21,24,39]. However, typical vein-like patterns are observed in the fractured sample under 5×10^{-3} s^{-1} (Fig. 5c2 and d2). It is well accepted that the temperature rise involves in the formation of vein-like patterns [40,41]. This indicates that temperature rise actually occurs during catastrophic fracture and thermal effect can be neglected during progressive sliding. In other words, we may conclude that the applied energy is fully dissipated by shear banding or progressive sliding when BMG samples undergo stable deformation.

Under dynamic loading, only shear band or crack branches form along the major cracks (Fig. 5a3 and a4). Crack opening can be observed within these branches (Fig. 5b3 and b4). This confirms that cracking occurs directly after single shear banding, and leads to unstable deformation manner at higher strain rate. The fracture surfaces exhibit relatively rough patterns with melting droplets under dynamic loading (Fig. 5c3-d3 and c4-d4), indicating a much stronger thermal effect involved during the cracking process. It seems that the applied energy under dynamic loading cannot be dissipated by multiple shear banding. Instead, crack opens directly from the single shear band and excessive release is achieved by local heating within cracks, which results in an unstable deformation manner.

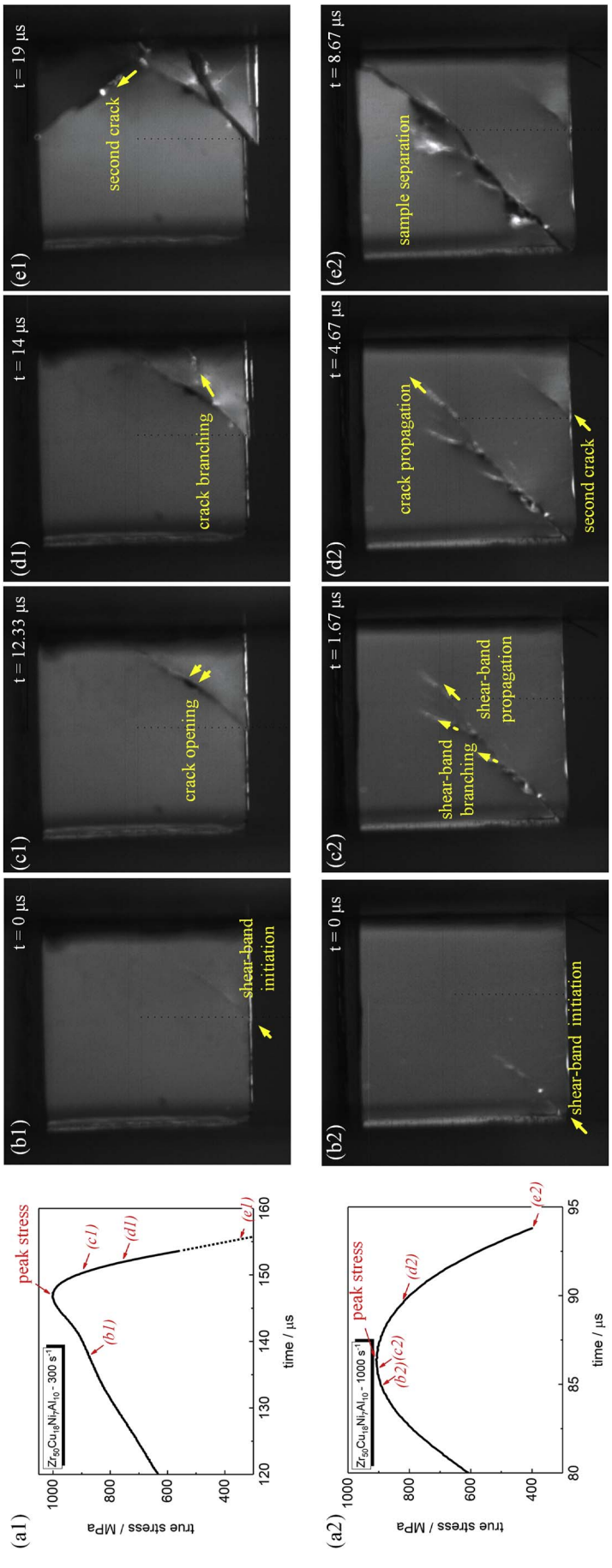

Fig. 4. Mechanical responses of Zr65-BMGs under (a1) 300 s^{-1} and (a2) 1000 s^{-1}. Characteristic shear banding and cracking behaviors of 300 s^{-1}, including (b1) formation of a single shear band, (c1) crack opening and propagation, (d1) crack bifurcation and (e1) formation of second crack; and (b2) – (e2) shear banding and cracking operations of 1000 s^{-1}.

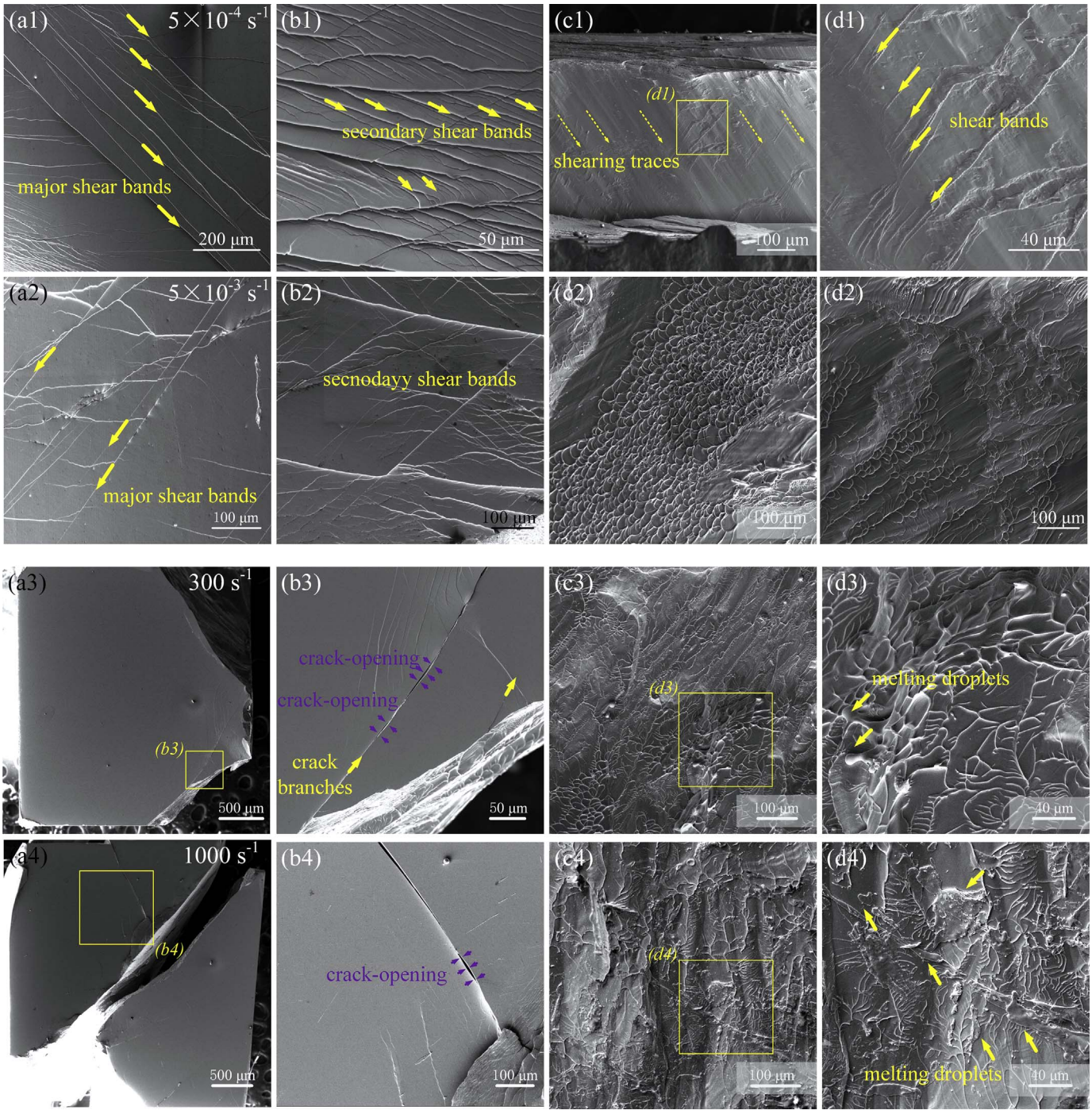

Fig. 5. Shear band and crack patterns of the fractured Zr65-BMG samples and corresponding fracture surfaces under (a1) – (d1) 5×10^{-4} s^{-1}, (a2) – (d2) 5×10^{-3} s^{-1}, (a3) – (d3) 300 s^{-1} and (a4) – (d4) 1000 s^{-1}.

3.3. Shear banding and cracking behaviors in brittle BMGs

Fig. 6 shows the stress-strain curves and characteristic shear banding behaviors of Zr50-BMGs under quasi-static compression. The stress-strain curves can be divided into elastic deformation stage and work-hardening stage, while strain-softening is absent in Zr50-BMGs (Fig. 6a1 and a2). It is worthy to note that multiple shear bands still form in the brittle BMGs during work-hardening (Fig. 6c1 and c2). Slip planes then form when the stress-strain curves turn to plateau (Fig. 6d1 and d2). However, this is followed by rapid sliding along the slip plane instead of progressive sliding. This indicates that Zr50-BMGs undergo unstable deformation once a slip plane forms, which corresponds to the absence of strain-softening. Compared to Zr65-BMGs, one can see multiple shear banding occurs in both ductile and brittle BMGs during work-hardening. The tendency of stable or unstable deformation under quasi-static loading in different compositions is governed by whether progressive or rapid sliding occurs along slip planes.

Fig. 7 shows the mechanical responses and characteristic deformation behaviors of Zr50-BMGs under dynamic compression. Similar to Zr65-BMGs, the stress-time curves of Zr50-BMGs only exhibit approximately elastic loading and direct softening (Fig. 7a1 and a2). Single shear banding and shear-band branching occur during the loading stage (Fig. 7b1-c1 and b2). A crack initiates directly from the single shear band (Fig. 7d1 and c2), and propagates to sample failure (Fig. 7e1 and

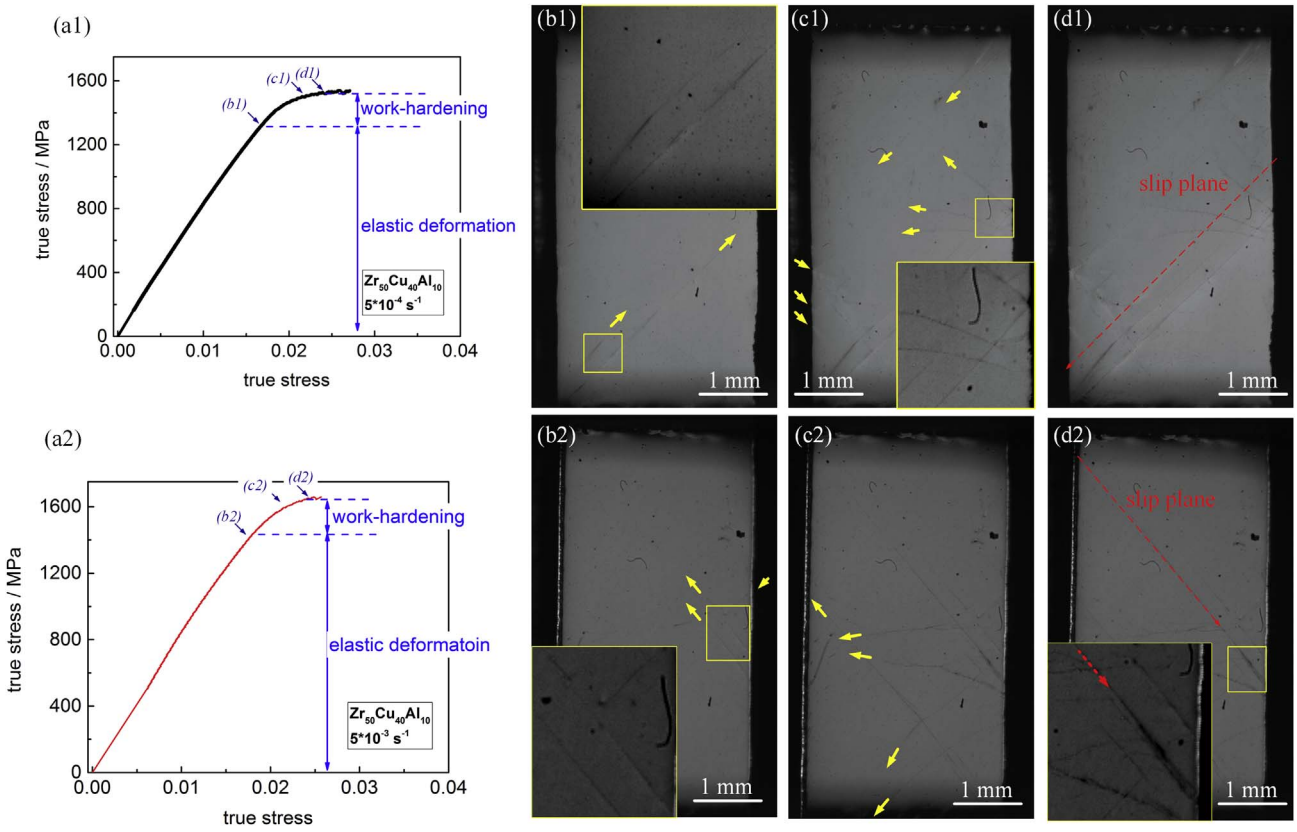

Fig. 6. Stress-strain curves of Zr50-BMGs under (a1) 5×10^{-4} s^{-1} and (a2) 5×10^{-3} s^{-1}, and corresponding shear banding behaviors under (b1) – (d1) 5×10^{-4} s^{-1} and (b2) – (d2) 5×10^{-3} s^{-1}.

d2-e2). Such deformation mode is consistent with the mode of Zr65-BMGs under dynamic loading. This demonstrates that both ductile and brittle BMGs undergo unstable deformation manner at high strain rate.

The shear band/crack patterns and fracture surfaces of Zr50-BMGs are further observed by SEM. The strain-rate effect on the shear band and crack patterns are similar to Zr65-BMGs, i.e., multiple shear bands are observed under quasi-static compression while cracks with branches observed under dynamic compression (Fig. 8a1-d1). However, the shear band density is lower than that of Zr65-BMGs under quasi-static loading (Fig. 5a1 and a2). Besides, secondary shear bands in Zr50-BMGs are much less than Zr65-BMGs (Fig. 5b1 and b2). As proposed above, the key reason for stable deformation is the alternant occurrence of secondary shear banding and progressive sliding. The absence of secondary shear banding in the brittle BMGs leads to much higher strain concentration within slip planes, which has a bigger chance to trigger unstable deformation once a slip plane forms. This is confirmed by the off-axial rupture along the slip plane (see the inset of Fig. 8b1). In addition, the fracture surfaces under quasi-static loading are covered by typical vein-like patterns (Fig. 8a2 and b2), which also indicates an unstable deformation during sliding. Under dynamic loading, shear band or crack branches are observed along the slip planes (Fig. 8c1 and d1). The fracture surfaces are covered by complicated patterns and several melting droplets are observed. This demonstrates a stronger excessive energy release.

The strain-rate effect on the deformation mode of Zr50-BMGs is a complicated issue. On the one hand, like Zr65-BMGs, the rate effect controls the transition from multiple shear banding to single shear banding during work-hardening. On the other hand, the rate effect on the tendency of stable or unstable deformation is not obvious in Zr50-BMGs. Unstable deformation occurs even when multiple shear bands form under quasi-static compression in Zr50-BMGs. Thus, the intrinsic properties of metallic glasses should be considered in the study of strain-rate effects.

4. Discussions

The observations presented in the above sections show that rate effect on the tendency of stable or unstable deformation actually originates from the distinct shear banding or cracking behaviors during the softening process. Under quasi-static compression, the plastic deformation of BMGs is accommodated by multiple shear banding and shear-dominated sliding along slip planes. The alternant occurrence of progressive sliding and secondary shear banding in ductile BMGs keep the samples undergoing a stable deformation manner and contribute to a considerable plasticity. Besides, the displacement of stable deformation decreases with increasing strain rate. However, rapid sliding occurs once a slip plane forms in brittle BMGs, which leads to unstable deformation. Under dynamic compression, crack opening from a single shear band occurs both in ductile and brittle BMGs.

As proposed above, local applied energy can be fully dissipated by shear banding during stable deformation, while the release of excessive energy can be observed during unstable deformation. In other words, the tendency of stable or unstable deformation is governed by the relationship between the applied energy and the dissipation energy through shear banding at a local softening area [42]. We concentrate on the local area and regard shear banding as an energy dissipation system [31]. Once the applied energy overcomes a critical plastic energy Γ_c dissipated in a shear band, BMGs tend to undergo unstable deformation such as crack propagation. On the contrary, when the applied energy is less that the critical dissipation energy, BMGs tend to undergo stable deformation like progressive sliding along the slip planes or secondary shear banding. Thus, the tendency can be characterized as a ratio of the local strain energy applied in a momentum diffusion zone E to the critical dissipated energy Γ_c within a shear band [23]. The plastic

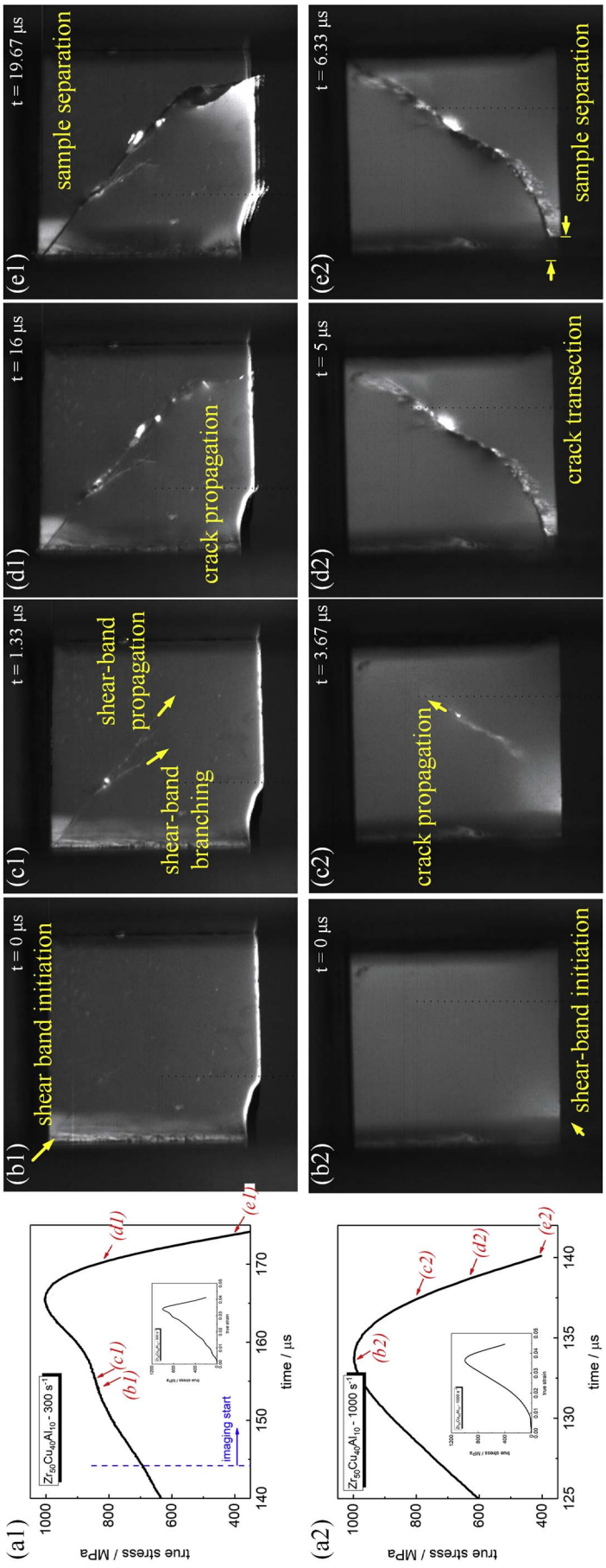

Fig. 7. Mechanical responses of Zr50-BMGs under (a1) 300 s^{-1} and (a2) 1000 s^{-1}. Characteristic shear banding and cracking behaviors under (b1) – (e1) 300 s^{-1} and (b2) – (e2) 1000 s^{-1}.

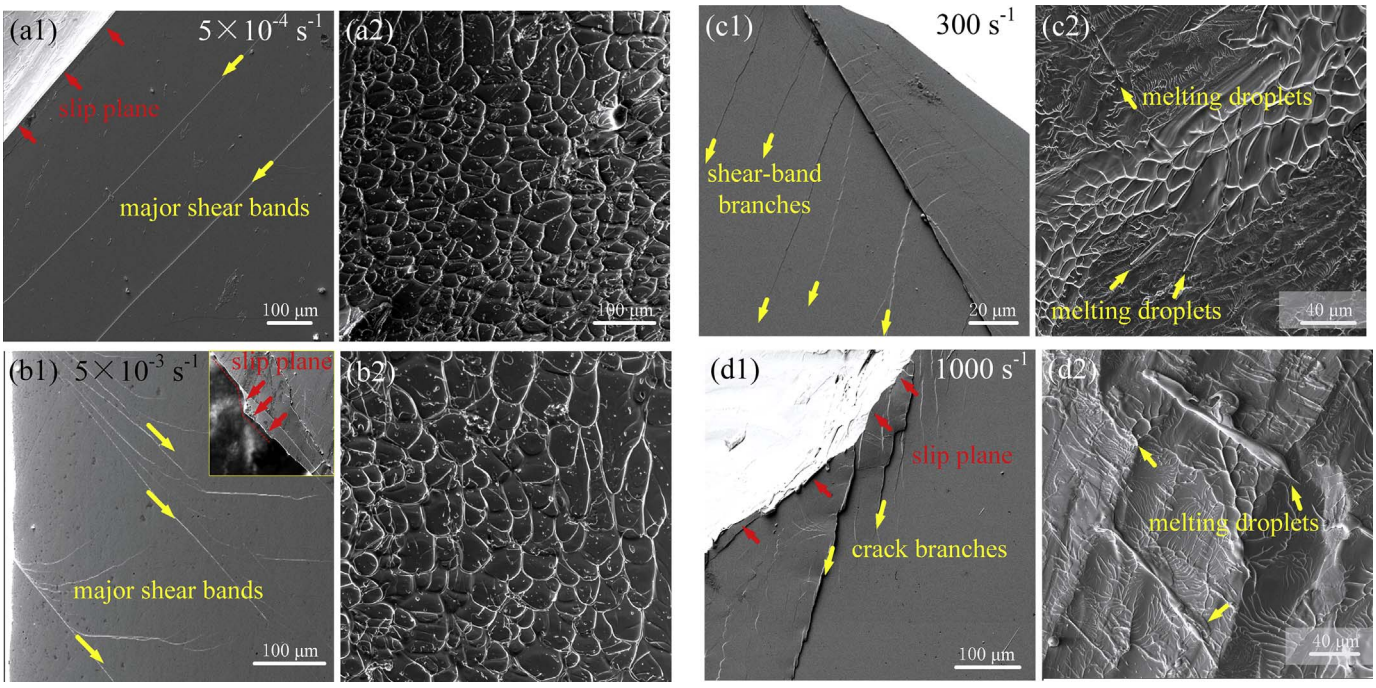

Fig. 8. Shear band and crack patterns and fracture surfaces of Zr50-BMGs under (a1) – (a2) 5×10^{-4} s^{-1}, (b1) – (b2) 5×10^{-3} s^{-1}, (c1) – (c2) 300 s^{-1} and (d1) – (d2) 1000 s^{-1}.

deformation of BMGs tends to be unstable if applied energy overcomes a critical plastic energy, i.e., $E/\Gamma_c > 1$. It tends to be stable when the ratio is smaller than 1 ($E/\Gamma_c < 1$). The critical dissipation energy per unit area Γ_c is proposed by Jiang and Dai [23,43] as

$$\Gamma_c = \left(\frac{9\rho D^3 \xi_c^6 \tau_y^3}{\dot{\gamma}_l R^5}\right)^{1/4} \tag{1}$$

where ρ is the density, D is the diffusion coefficient of free-volume, ξ_c is the increase of free-volume concentration within a shear band, $\dot{\gamma}_l$ is the local shear strain rate, and R is the local dilatation.

The elastic strain energy applied in a momentum diffusion zone under quasi-static compression E_s can be characterized as [23].

$$E_s = \frac{\tau_{ys}^2 \delta_B}{2\mu}\sqrt{\frac{\chi}{D}} \tag{2}$$

and the strain energy under dynamic compression E_d can be characterized as [23].

$$E_d = \frac{\tau_{yd}^2 \delta_B}{2\mu}\sqrt{\frac{\tau_{yd}}{\rho \dot{\gamma}_l D}} \tag{3}$$

where τ_{ys} and τ_{yd} are the shear yielding strength under quasi-static compression and dynamic compression, δ_B is the shear-band width, μ is the shear modulus, and χ is the heat diffusion coefficient. The parameters are listed in Table 1.

It is worthy to note that the level of free-volume diffusion D varies from different compositions. Although the free-volume diffusion is difficult to be measured experimentally, it shows a negative dependence of shear band spacing by Chen [47] and Zeng [23]. When the level of free-volume diffusion is relatively lower, the free-volume in BMGs is harder to diffuse to surrounding regions, causing a larger shear band spacing. On the contrary, a higher free-volume diffusion level would lead to a smaller shear band spacing. In our experiments, the shear banding spacing of Zr65-BMGs is smaller than that of Zr50-BMGs, which implies a larger D in Zr65-BMGs. Here we set $D = 2 \times 10^{-9}$ m^2s^{-1} in Zr65-BMGs, and $D = 2 \times 10^{-10}$ m^2s^{-1} in Zr50-BMGs. In addition, the strain rate in Eqs.(1) and (3) stands for local strain rate. Zhang et al. proposed [48] that the macroscopic strain rate from quasi-static to dynamic loading corresponds to the range from 10^3 s^{-1} to 10^9 s^{-1}.

Table 1
Parameters for strain energy and critical dissipation energy.

Materials	τ_{ys}/GPa	τ_{yd}/GPa	μ/GPa	δ_B/nm	ρ/gcm^{-3}
$Zr_{50}Cu_{40}Al_{10}$	1.156	0.825	34	10 [44,45]	6.714
$Zr_{65}Cu_{18}Ni_7Al_{10}$	1.015	0.753	31	10	6.834

Materials	χ/m^2s^{-1}	D/m^2s^{-1}	R	ξ_c
$Zr_{50}Cu_{40}Al_{10}$	3×10^{-6} [46]	10^{-10}–10^{-8} [43]	0.0027 [23]	3.6% [42]
$Zr_{65}Cu_{18}Ni_7Al_{10}$				

Fig. 9a1 and a2 show the ratios of the local strain energy to the critical dissipation energy in a shear band under quasi-static E_s/Γ_c and under dynamic compression E_d/Γ_c, respectively. The local strain rate $\dot{\gamma}_l = 10^6\, s^{-1}$ is regarded as the transition from quasi-static to dynamic loading. Under quasi-static loading (Fig. 9a), the ratio of Zr65-BMG remains smaller than 1, which indicates that the locally applied energy can be fully dissipated by shear banding or progressive sliding. This confirms the stable deformation manner in Zr65-BMGs at lower strain rate (Fig. 3). Furthermore, the ratio is approaching to 1 in Zr65-BMGs with increasing strain rate. The chance of unstable deformation becomes bigger when the ratio reaches 1. This might explain why the displacement of stable sliding decreases with increasing loading rate. The ratio of Zr50-BMGs remains larger than 1 under quasi-static loading, which is in line with an unstable deformation manner (Fig. 6). Under dynamic compression (Fig. 9b), the ratios are much larger than 1 both in Zr65-BMGs and Zr50-BMGs. This corresponds to unstable deformation in the form of cracking from single shear banding.

Comparing Fig. 9a and b, a jump in the ration can be observed from quasi-static to dynamic strain rate. The jump might be attributed to a transition from shear-dominated sliding under quasi-static loading to cracking-dominated fracture under dynamic loading. A critical strain rate may exist to control this transition. Li et al. [24] estimated such strain rate to be about 450 s^{-1}, while our previous study proposed that the critical value was in the range from 10^1 s^{-1} to 10^2 s^{-1}. The examination of the critical strain rate needs further investigation at

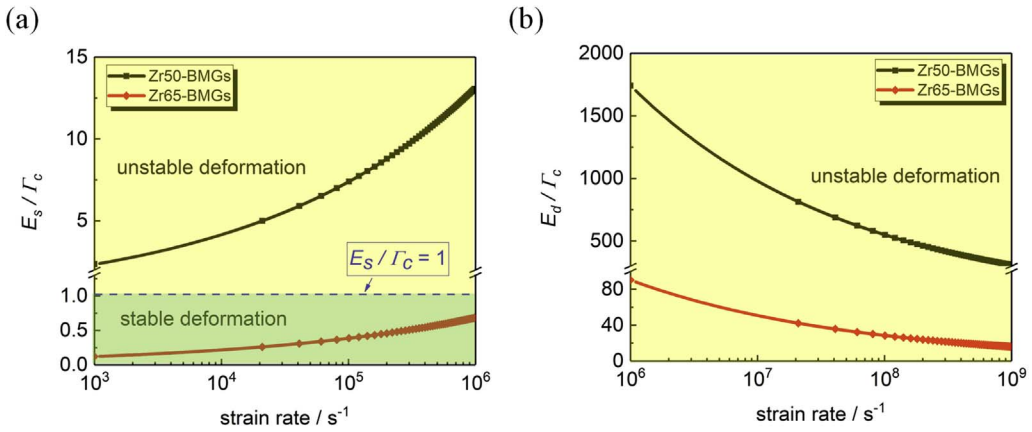

Fig. 9. Ratio of local elastic strain energy and critical dissipated energy within a shear band under (a) quasi-static compression and (b) dynamic compression.

intermediate strain rate. Besides, the ratio gradually decreases with increasing strain rate under dynamic loading (Fig. 9b). This predicates a possibly stable deformation at a super high strain rate. Lu et al. [49] reported a ductile fracture in Zr50-BMGs in the flyer-plate impact experiments, which is consistent with our prediction.

5. Conclusions

The rate effect on the deformation mode of BMGs are investigated via real-time photographing, and a comparative study is performed between ductile and brittle BMGs. The plastic deformation of BMGs is accommodated by multiple shear banding and sliding along slip planes under quasi-static compression. Ductile BMGs tends to undergo stable deformation in the form of progressive sliding along slip planes. In brittle BMGs, rapid sliding occurs once a slip plane forms, which leads to unstable deformation manner even at lower strain rate. Under dynamic compression, both ductile and brittle BMGs tend to undergo unstable deformation via cracking from a single shear band. The tendency of stable or unstable deformation shows a direct correlation to energy release in the local shear banding area. A model based on the ratio of applied strain energy to critical dissipation energy in a shear band has well characterized our findings. In addition, the model predicts a critical rate controls the transition of deformation mode at intermediate strain rate, and possible stable deformation at super high loading rate.

Acknowledgements

This work is sponsored by the Innovation Foundation for Doctor Dissertation of Northwestern Polytechnical University (NPU) (No. CX201707). The authors thank the supports by National Science Foundation (Nos. 11572260, 11527803 and 11790292). Thanks for the materials supports from Dr. C. Zhang and Dr. J.C. Qiao from NPU. Thanks for the language modifications by Mr. S. Zakir.

Appendix A. Supplementary data

Supplementary data related to this article can be found at http://dx.doi.org/10.1016/j.intermet.2018.01.020.

References

[1] A.L. Greer, Y.Q. Cheng, E. Ma, Shear bands in metallic glasses, Mater. Sci. Eng. R Rep. 74 (4) (2013) 71–132 https://doi.org/10.1016/j.mser.2013.04.001.
[2] Y.H. Liu, C.T. Liu, A. Gali, et al., Evolution of shear bands and its correlation with mechanical response of a ductile $Zr_{55}Pd_{10}Cu_{20}Ni_5Al_{10}$ bulk metallic glass, Intermetallics 18 (8) (2010) 1455–1464 https://doi.org/10.1016/j.intermet.2010.03.037.
[3] P. Tao, Y. Yang, X. Bai, et al., The relationship between shear bands and deformability in bulk metallic glasses, J. Alloy. Comp. 536 (2012) 226–230 https://doi.org/10.1016/j.jallcom.2012.04.061.
[4] R.T. Qu, Z.Q. Liu, G. Wang, et al., Progressive shear band propagation in metallic glasses under compression, Acta Mater. 91 (2015) 19–33 https://doi.org/10.1016/j.actamat.2015.03.026.
[5] M. Zhang, Y. Chen, L.H. Dai, An index of shear banding susceptibility of metallic glasses, Intermetallics 71 (2016) 12–17 https://doi.org/10.1016/j.intermet.2015.11.010.
[6] G.N. Yang, B.A. Sun, S.Q. Chen, et al., The multiple shear bands and plasticity in metallic glasses: a possible origin from stress redistribution, J. Alloy. Comp. 695 (2017) 3457–3466 https://doi.org/10.1016/j.jallcom.2016.12.012.
[7] B. Shi, Y. Xu, C. Li, et al., Evolution of free volume and shear band intersections and its effect on hardness of deformed $Zr_{64.13}Cu_{15.75}Ni_{10.12}Al_{10}$ bulk metallic glass, J. Alloy. Comp. 669 (2016) 167–176 https://doi.org/10.1016/j.jallcom.2016.01.239.
[8] D.P. Wang, B.A. Sun, X.R. Niu, et al., Mutual interaction of shear bands in metallic glasses, Intermetallics 85 (2017) 48–53 https://doi.org/10.1016/j.intermet.2017.01.015.
[9] S. Pauly, M.H. Lee, D.H. Kim, et al., Crack evolution in bulk metallic glasses, J. Appl. Phys. 106 (10) (2009) 103518 https://doi.org/10.1063/1.3259418.
[10] Y.-Y. Zhao, G. Zhang, D. Estévez, et al., Evolution of shear bands into cracks in metallic glasses, J. Alloy. Comp. 621 (2015) 238–243 https://doi.org/10.1016/j.jallcom.2014.09.205.
[11] R. Maaß, P. Birckigt, C. Borchers, et al., Long range stress fields and cavitation along a shear band in a metallic glass: the local origin of fracture, Acta Mater. 98 (2015) 94–102 https://doi.org/10.1016/j.actamat.2015.06.062.
[12] R.T. Qu, S.G. Wang, X.D. Wang, et al., Revealing the shear band cracking mechanism in metallic glass by X-ray tomography, Scripta Mater. 133 (2017) 24–28 http://doi.org/10.1016/j.scriptamat.2017.02.018.
[13] R. Narasimhan, P. Tandaiya, I. Singh, et al., Fracture in metallic glasses: mechanics and mechanisms, Int. J. Fract. 191 (1) (2015) 53–75, http://dx.doi.org/10.1007/s10704-015-9995-3.
[14] Y.H. Liu, G. Wang, R.J. Wang, et al., Super plastic bulk metallic glasses at room temperature, Science 315 (5817) (2007) 1385–1388, http://dx.doi.org/10.1126/science.1136726.
[15] B.A. Sun, H.B. Yu, W. Jiao, et al., Plasticity of ductile metallic glasses: a self-organized critical state, Phys. Rev. Lett. 105 (3) (2010) 035501, http://dx.doi.org/10.1103/physrevlett.105.035501.
[16] W. Yang, B. Sun, Y. Zhao, et al., Non-repeatability of large plasticity for Fe-based bulk metallic glasses, J. Alloy. Comp. 676 (2016) 209–214 https://doi.org/10.1016/j.jallcom.2016.03.169.
[17] T. Mukai, T.G. Nieh, Y. Kawamura, et al., Effect of strain rate on compressive behavior of a $Pd_{40}Ni_{40}P_{20}$ bulk metallic glass, Intermetallics 10 (11) (2002) 1071–1077 https://doi.org/10.1016/S0966-9795(02)00137-1.
[18] G. Subhash, R.J. Dowding, L.J. Kecskes, Characterization of uniaxial compressive response of bulk amorphous Zr–Ti–Cu–Ni–Be alloy, Mater. Sci. Eng. 334 (1) (2002) 33–40 https://doi.org/10.1016/S0921-5093(01)01768-3.
[19] Y.F. Xue, H.N. Cai, L. Wang, et al., Effect of loading rate on failure in Zr-based bulk metallic glass, Mater. Sci. Eng. 473 (1–2) (2008) 105–110 https://doi.org/10.1016/j.msea.2007.04.044.
[20] M. Song, Y. Li, Y. He, Effect of strain rate on the compressive behaviour of a $Zr_{56}Al_{10.9}Ni_{4.6}Cu_{27.8}Nb_{0.7}$ bulk metallic glass, Phil. Mag. Lett. 90 (10) (2010) 763–770, http://dx.doi.org/10.1080/09500839.2010.507175.
[21] W. Zheng, Y.J. Huang, G.Y. Wang, et al., Influence of strain rate on compressive deformation behavior of a Zr-Cu-Ni-Al bulk metallic glass at room temperature, Metall. Mater. Trans. 42 (6) (2011) 1491–1498, http://dx.doi.org/10.1007/s11661-011-0632-0.
[22] J. Liu, V.P.W. Shim, La-based bulk metallic glass failure analysis under static and dynamic loading, Int. J. Impact Eng. 60 (2013) 37–43 https://doi.org/10.1016/j.ijimpeng.2013.04.004.
[23] F. Zeng, Y. Chen, M.Q. Jiang, et al., Dynamic fragmentation induced by network-like shear bands in a Zr-based bulk metallic glass, Intermetallics 56 (2015) 96–100

https://doi.org/10.1016/j.intermet.2014.09.008.
[24] M.C. Li, M.Q. Jiang, S. Yang, et al., Effect of strain rate on yielding strength of a Zr-based bulk metallic glass, Mater. Sci. Eng. 680 (2017) 21–26 https://doi.org/10.1016/j.msea.2016.10.081.
[25] L.C. Zhang, F. Jiang, Y.L. Zhao, et al., Stable shear of $Cu_{46}Zr_{47}Al_7$ bulk metallic glass alloy by controlling temperature rise, Mater. Sci. Eng. 527 (16) (2010) 4122–4127 https://doi.org/10.1016/j.msea.2010.03.032.
[26] Y.H. Li, W. Zhang, C. Dong, et al., Effects of cryogenic temperatures on mechanical behavior of a $Zr_{60}Ni_{25}Al_{15}$ bulk metallic glass, Mater. Sci. Eng. 584 (2013) 7–13 https://doi.org/10.1016/j.msea.2013.06.063.
[27] G. Li, M.Q. Jiang, F. Jiang, et al., The ductile to brittle transition behavior in a Zr-based bulk metallic glass, Mater. Sci. Eng. 625 (2015) 393–402 https://doi.org/10.1016/j.msea.2014.11.088.
[28] S.J. Wu, X.D. Wang, R.T. Qu, et al., Gradual shear band cracking and apparent softening of metallic glass under low temperature compression, Intermetallics 87 (2017) 45–54.
[29] F.F. Wu, W. Zheng, S.D. Wu, et al., Shear stability of metallic glasses, Int. J. Plast. 27 (4) (2011) 560–575 https://doi.org/10.1016/j.ijplas.2010.08.004.
[30] Z.F. Zhang, H. Zhang, X.F. Pan, et al., Effect of aspect ratio on the compressive deformation and fracture behaviour of Zr-based bulk metallic glass, Phil. Mag. Lett. 85 (10) (2005) 513–521, http://dx.doi.org/10.1080/09500830500395237.
[31] Z. Han, W.F. Wu, Y. Li, et al., An instability index of shear band for plasticity in metallic glasses, Acta Mater. 57 (5) (2009) 1367–1372 https://doi.org/10.1016/j.actamat.2008.11.018.
[32] Z.F. Zhang, J. Eckert, L. Schultz, Difference in compressive and tensile fracture mechanisms of $Zr_{59}Cu_{20}Al_{10}Ni_8Ti_3$ bulk metallic glass, Acta Mater. 51 (4) (2003) 1167–1179 https://doi.org/10.1016/S1359-6454(02)00521-9.
[33] J. Caris, J.J. Lewandowski, Pressure effects on metallic glasses, Acta Mater. 58 (3) (2010) 1026–1036 https://doi.org/10.1016/j.actamat.2009.10.018.
[34] B.A. Sun, C.T. Liu, Y. Yang, Rate dependence of serrated flow and its effect on shear stability of bulk metallic glasses, J. Iron. Steel Res. Int. 23 (1) (2016) 24–30 https://doi.org/10.1016/S1006-706X(16)30006-1.
[35] W.H. Jiang, M. Atzmon, Room-temperature flow in a metallic glass – strain-rate dependence of shear-band behavior, J. Alloy. Comp. 509 (27) (2011) 7395–7399 https://doi.org/10.1016/j.jallcom.2011.04.041.
[36] Y. Xue, L. Wang, X. Cheng, et al., Strain rate dependent plastic mutation in a bulk metallic glass under compression, Mater. Des. 36 (2012) 284–288 https://doi.org/10.1016/j.matdes.2011.11.025.
[37] R. Sarmah, G. Ananthakrishna, B.A. Sun, et al., Hidden order in serrated flow of metallic glasses, Acta Mater. 59 (11) (2011) 4482–4493 https://doi.org/10.1016/j.actamat.2011.03.071.
[38] B.A. Sun, S. Pauly, J. Hu, et al., Origin of intermittent plastic flow and instability of shear band sliding in bulk metallic glasses, Phys. Rev. Lett. 110 (22) (2013) 225501.
[39] J. Li, Y.W. Wang, J. Yi, et al., Strain-energy transport during fracture of metallic glasses, J. Alloy. Comp. 680 (2016) 43–53 http://doi.org/10.1016/j.jallcom.2016.04.117.
[40] R.T. Qu, Z.F. Zhang, Compressive fracture morphology and mechanism of metallic glass, J. Appl. Phys. 114 (19) (2013) 193504, http://dx.doi.org/10.1063/1.4830029.
[41] B.A. Sun, W.H. Wang, The fracture of bulk metallic glasses, Prog. Mater. Sci. 74 (2015) 211–307 https://doi.org/10.1016/j.pmatsci.2015.05.002.
[42] J. Pan, Q. Chen, L. Liu, et al., Softening and dilatation in a single shear band, Acta Mater. 59 (13) (2011) 5146–5158 https://doi.org/10.1016/j.actamat.2011.04.047.
[43] M.Q. Jiang, L.H. Dai, Shear-band toughness of bulk metallic glasses, Acta Mater. 59 (11) (2011) 4525–4537 https://doi.org/10.1016/j.actamat.2011.03.075.
[44] Y. Zhang, A.L. Greer, Thickness of shear bands in metallic glasses, Appl. Phys. Lett. 89 (7) (2006) 071907, http://dx.doi.org/10.1063/1.2336598.
[45] Q.P. Cao, J.F. Li, Y.H. Zhou, et al., Microstructure and microhardness evolutions of $Cu_{47.5}Zr_{47.5}Al_5$ bulk metallic glass processed by rolling, Scripta Mater. 59 (6) (2008) 673–676 https://doi.org/10.1016/j.scriptamat.2008.05.023.
[46] D.B. Miracle, A. Concustell, Y. Zhang, et al., Shear bands in metallic glasses: size effects on thermal profiles, Acta Mater. 59 (7) (2011) 2831–2840 https://doi.org/10.1016/j.actamat.2011.01.022.
[47] Y. Chen, M.Q. Jiang, L.H. Dai, Collective evolution dynamics of multiple shear bands in bulk metallic glasses, Int. J. Plast. 50 (2013) 18–36 https://doi.org/10.1016/j.ijplas.2013.03.010.
[48] H. Zhang, S. Maiti, G. Subhash, Evolution of shear bands in bulk metallic glasses under dynamic loading, J. Mech. Phys. Solid. 56 (6) (2008) 2171–2187 https://doi.org/10.1016/j.jmps.2008.01.008.
[49] L. Lu, C. Li, W.H. Wang, et al., Ductile fracture of bulk metallic glass $Zr_{50}Cu_{40}Al_{10}$ under high strain-rate loading, Mater. Sci. Eng. 651 (2016) 848–853 https://doi.org/10.1016/j.msea.2015.11.040.